2022-12-10

Hydroxyapatite-activated seaweed biochar for enhanced remediation of fluoride contaminated soil at various pH ranges

Moirana, Ruth

Elsevier

Provided with love from The Nelson Mandela African Institution of Science and Technology

Hydroxyapatite-activated seaweed biochar for enhanced remediation of fluoride contaminated soil at various pH ranges

Ruth Lorivi Moirana [a,*], Josephine Mkunda [a], Revocatus Machunda [a], Marcos Paradelo [b], Kelvin Mtei [a]

[a] *School of Material, Energy, Water, and Environmental Sciences, The Nelson Mandela African Institute of Science and Technology, P.O. Box 447, Nambala, Arusha 23311, Tanzania*
[b] *Natural Resources Institute, University of Greenwich, Central Avenue, Chatham Maritime, Kent ME4 4TB. UK*

ARTICLE INFO

ABSTRACT

This study investigated the defluoridation efficiency of hydroxyapatite-activated seaweed (*Eucheuma Cottonii*) biochar (HSB) at various soil pH ranges (3–11) while monitoring the impact of contact time (30 min - 2.5 h), adsorbent dosage (0.1–0.5 g) as well as the initial fluoride concentration and compare its performance to its respective seaweed biochar (SB). Activation of SB with the hydroxyapatite lead to a shift in its point-zero-charge (pH_{PZC}) from 6 to 7.4 broadening its defluoridation pH range from a solitary 5 to amid 3 through 11. The fluoride adsorption mechanism was found to follow both Langmuir ($R^2 = 0.956$) and Freundlich ($R^2 = 0.942$) isotherm models with a maximum defluoridation capacity of 3.03 mg/g equivalent to the defluoridation efficiency of 79%. This is accounted to the existence of soil ions, SB active sites, and the attached hydroxyapatite, as fluoride adsorption sites each exhibiting a dissimilar fluoride removal mechanism. Therefore, the HSB could be a promising adsorbent for fluoride removal in the fluoride contaminated agricultural soils of inclusive pH ranges.

1. Introduction

Exposure to low fluoride concentration of < 1.5 mg/L is beneficial for stronger bones and teeth (Moirana et al., 2021) but prolonged exposure to concentrations higher than 3 mg/L leads to skeletal fluorosis and gastrointestinal problems in animals, particularly human beings (Hegde et al., 2020). Normally, fluorosis is associated with fluoride in drinking water (Rizzu et al., 2020), and exposure to fluoride through other sources such as food and air has been overlooked. This has led to the establishment of different techniques specific to drinking water. In 1978, Olsson discovered symptoms of fluorosis in 18% of the population in Ethiopia with fluoride concentration in drinking water as low as 0.2 - 0.3 mg/L (Olsson, 1978). Another study by Ibrahim and coworkers (1995) investigated the prevalence of fluorosis in children in Sudan consuming drinking water with 0.25 mg/L fluoride of which 91% of the children revealed the symptoms of fluorosis (Ibrahim et al., 1995). The results from these studies and many others demonstrated the availability of different fluoride exposure sources besides drinking water (Malde et al., 1997).

One other major source of fluoride exposure is soil which transfers fluoride to plants and animals. Plants absorb the fluoride in the soil-water interface through the roots (Rizzu et al., 2020). Therefore, if the soil or irrigation water contains fluoride, the plant roots will likely absorb fluoride ions as part of the soil solution (Hong et al., 2016; Moirana et al., 2021). Plants/crops accumulate different fluoride concentration levels. A study conducted by Arnesen (1997) revealed that white clover (*Trifolium repens)* could not accumulate fluoride more than 30 mg/kg compared to the ryegrass (*Lolium multiflorium*) which could absorb up to 50 mg/kg in a high fluoride polluted soil (Arnesen, 1997). In another study, Rizzu et al. (2020) revealed that kale (*Brassica* sp. pl.) could accumulate up to 14.2 mg/kg, higher than beans (*Phaseolus vulgaris* L.) with 11.3 mg/kg, maize (*Zea mays* L.) with 8 mg/kg and tomato (*Lycopersicon esculentum* Mill.) with 11.4 mg/kg (Rizzu et al., 2020). The soil fluoride uptake and accumulation by plants not only affect the quality and quantity of crop production but expose human beings and other life forms within the ecosystem and the food chain to fluoride (Zuo et al., 2018; Rizzu et al., 2020).

Bio-adsorbents have been used for defluoridation purposes (Bashir et al., 2015). These materials contain functional groups such as hydroxyl, carboxyl, thiol, amine, and sulfate, which can be modified to

---

acquire efficient defluoridation capacities (Evangeline and Pragasam, 2015). There are several bio-adsorbents reported for water defluoridation (Tomar et al., 2014; Bashir et al., 2015; Nehra et al., 2020; Qiu et al., 2020), but the literature for soil remediation using bio-adsorbents, particularly those derived from seaweed is still limited. This could be driven by its low efficiency, mainly in alkaline conditions (Marcus, 1991) which is of great concern since agricultural soils could have pH from slightly acidic to strong alkaline.

While agricultural soils could have a variety of pH range, most reported biochar adsorbents efficient fluoride removal only takes place under acidic conditions (5.5 -6.5) (Marcus, 1991) which Marcus (1991) and Liyuan et al. (2013) argues to be attributed by excessive hydration energy of fluoride (-465 kJ/mol) competing with that of hydroxyl ions in the adsorbents (-430 kJ/mol) making the inner-sphere coordination between fluoride and the biochar almost impossible to happen under neutral to alkaline conditions (Montazeri et al., 2011; Chai et al., 2013). On the other hand, hydroxyapatite ($Ca_5(PO_4)_3OH$) which is a salt of calcium phosphate is known for its higher fluoride affinity forming highly stable fluorapatite ($Ca_5(PO_4)_3F$) which is a part of its being environmentally friendly, but its usage in large scale is limited by its cost of production (McQuaker and Gurney, 1977; Mukherjee et al., 2018). Therefore, a challenge remains finding a cost-effective adsorbent with high efficiency at a wide pH range.

The present study explores the possibility of using a cost-effective seaweed biochar that has been activated using hydroxyapatite towards fluoride removal from the fluoride contaminated agricultural soil at different pH ranges. The study further compares the performance of the hydroxyapatite activated seaweed derived biochar (HSB) to that of its original seaweed biochar (SB) while investigating other experimental conditions such as adsorbent dosage, contact time and adsorption mechanisms using adsorption models.

2. Materials and methods

2.1. Adsorbent material

The seaweed *Eucheuma cottonii* was obtained at the beaches of the Indian ocean in the Tanga region (Tanzania). The seaweed was thoroughly washed with distilled water, air-dried, and ground into a fine powder using a mechanical grinder. The experimental soil was collected from Ngarenanyuki ward, Arusha (Tanzania) which is a place known to contain significant amounts of fluoride in both soil and water. The powdered seaweed was pyrolyzed in a tube furnace at 450 °C for 2 h under continuous N_2 flow. The temperature ramp was maintained at 10 °C/min up until the desired temperature was reached. The pyrolysis temperature was selected in order to recover high biochar yield and moderate cation exchange capacity (CEC) (Liang et al., 2016). Thereafter, the carbonaceous materials which were now seaweed biochar (SB) were recovered. To facilitate the reaction, SB was first dipped with 1M HCl, washed with distilled water followed by dipping into 1M NaOH solution, and thereafter rinsing it several times (Qiu et al., 2020).

The hydroxyapatite-activated seaweed-derived biochar (HSB) was prepared by taking 5 g seaweed biochar (SB) and dissolved in a 200 mL solution of 1M diammonium phosphate $(NH_4)_2PO_4$, stirred at 200 rpm for 12 h. After the 12 h, the SB was filtered out by centrifuging at 4000 rpm for 15 min, rinsed and transferred to a 1.67 M solution of $Ca(NO_3)_2$ maintained at a minimum pH of 10 using ammonia solution (NH_3OH). The contents were allowed to mature by stirring for 24 h at room temperature (24 ± 2 °C). Afterward, the hydroxyapatite-activated seaweed biochar (HSB) was separated from its mother solution by centrifugation and rinsed several times with distilled water. The material was then oven-dried at 70 °C for 2 days and crushed into a fine powder using a mortar and pestle.

2.2. Characterization and analysis

The scanning electron microscope (SEM-EDX) was used to observe the morphology of the hydroxyapatite particles attached to the SB, and XRD was used to capture the crystal structure of the composite before and after activation with hydroxyapatite and after fluoride adsorption. The Point-zero-charge (pHzpc) of the composite material was determined using the pH drift method. The pH and electric conductivity (EC) of the experimental soil was measured using the same instrument (Orion 5Star). The carbon (C), hydrogen (H), nitrogen (N), sulphur (S) and oxygen (O) were determined using a micro-element analyzer. For the analysis of moisture content, 2 g of the air-dried seaweed and seaweed biochar were oven dried at 105 °C for 3 h, stored in the desiccator and weighed when cooled to room temperature. The ash content was measured by burning a 2 g samples (dried seaweed and seaweed biochar) at 850 °C for 1.5 h and the volatile matter content was measured by burning the samples at 970 °C for 15 min. The contents were calculated as the difference between the initial and final weights.

2.3. Fluoride determination

Total fluoride was quantified based on McQuaker et al. (1977) procedure (McQuaker and Gurney, 1977). The 0.5 g of the sample was put into the crucibles and moisturized with 5 ml of distilled water (DW). Thereafter, 6 mL of concentrated NaOH (17 M) was mixed and placed into the oven at 150 °C for 1 h. The samples were then moved into the muffle furnace set at 600 °C for 30 min and left to cool to room temperature. Distilled water was added for the dissolution of the NaOH cake and then moved to the 100 mL centrifuge tubes where pH was adjusted to 8-9 by concentrated HCl followed by fluoride quantification.

For the determination of water-soluble fluoride (Ws-F), 2.5 g of the sample was added into a 50 mL falcon tube followed by the addition of 25 mL DW. The samples were kept shaking in the incubator set at 60 °C for 30 min. Next, the samples were shaken and centrifuged and the supernatant was collected for measurements. The amount of fluoride present in the soil before and after the addition of the composite material was measured by fluoride ion-selective electrode (F- ISE) using total ion strength adjustment buffer (TISAB II) at a 1:1 with the analyte sample. The fluoride removal efficiency and defluoridation capacity of the composite were calculated as presented by Eqs. (1) and (2).

$$Fluoride\ removal(\%) = ((C_i - C_e) / C_i) * 100 \qquad (1)$$

$$q_e = (C_i - C_e)/W)V \qquad (2)$$

where qe is defluoridation capacity (mg/g), Ci is the initial fluoride concentration (mg/L), C_e is the equilibrium fluoride concentration (mg/L), W is the weight of adsorbent added (g) and V is the volume of the solution (L)

2.4. Experimental set-up

The natural fluoride-containing soil with the initial fluoride concentration (C_i) of 103 ± 3 mg/kg was used to study the influence of adsorbent dosage, contact time, and pH on the defluoridation capacity of the HSB adsorbent. The impact of initial fluoride concentration on HSB defluoridation capacity was studied by spiking the soil with 25, 50, 75, and 100 mg/L fluorides in form of NaF and incubating for 1 month before the experiment. The selected properties of the soil used for this

Table 1
The selected properties of the experimental soil.

Sand (%)	Clay (%)	Silt (%)	OM (%)	pH	Ws-F (mg/kg)	Tot-F (mg/kg)
75.4	6.4	18.2	2.5 ± 0.1	9 ± 1.3	103.1 ± 3	± 36

study are presented in Table 1 and the soil analysis was conducted as per our previous study (Moirana et al., 2021).

In each of the batch experiments, 5 g of the soil sample was mixed with the selected adsorbent dose, moistened, and incubated for 12 h before the test experiment begins. Five different adsorbent dosages were investigated for soil fluoride lock-off efficiency (0.1, 0.2, 0.3, 0.4, and 0.5 g together with the controls), the kinetic study comprised of 30 min, 1,1.5, 2, and 2.5 h contact time whereas the impact of pH was investigated from (pH 3-11) at an interval of 2. To study the performance of the adsorbent at various pH ranges, the contact time was maintained 1 h while stirring at 100 rpm, adsorbent dosage used was 0.2 g and at room temperature (25 ± 2 °C). All the experiments were conducted in triplicates and the results are reported as mean values.

3. Results and discussion

3.1. Characterization

The moisture, ash and volatile matter content of the seaweed was found to be 5.98 ± 1%, 24.3 ± 1%, and 49.1 ± 2% compared to its biochar which was 0.9 ± 0.3%, 22.9 ± 1%, and 32 ± 2%, respectively. The moisture, ash and volatile matter of SB biochar obviously decreased compared to dried seaweed matter which is crucial for increasing the absorption surface area of the biochar. The amount of fixed carbon, C, H, N, S and O for seaweed was 19.3 ± 4, 48.2 ± 1%, 7 ± 0%, 1.1 ± 0%, 0.9 ± 0%, and 41 ± 2% whereas for seaweed biochar was 43.7 ± 1, 56.2 ± 2%, 6 ± 1%, 1.2 ± 0%, 1.3 ± 0%, 21 ± 2%, respectively. Both seaweed and its biochar had high contents of C and O but carbonization process lead to an increment of C and decrement if O. the increment in carbon is influenced by the pyrolysis process which leads to a more concentrated carbon material whereas decrement of O highlights the presence of aromatic compounds in the seaweed.

The XRD patterns of SB, HSB, and F-SHB are presented in Fig. 1. The SB represented by a black line is characterized by a significant amount of amorphous materials and crystalline peaks of calcite ($CaCO_3$) at 23°, 29°, 36°, 40°,43.5°,48°, and 49° 2θ, quartz (SiO_2) at 21° and 26.5° 2θ and calcium hydroxide ($Ca(OH)_2$) at 34° 2θ. Activation to HSB represented by a red line, reveals additional peaks to the SB at 31° – 35° 2θ.

The additional peaks observed matches with the hydroxyapatite ($Ca_5(PO_4)_3(OH)_2$) peaks synthesized during the addition of diammonium phosphate (($NH_4)_2PO_4$) and calcium nitrate ($Ca(NO_3)_2$) into the seaweed biochar and therefore confirms the formation of hydroxyapatite in the adsorbent. The width of the peaks suggests that the attached hydroxyapatite in the SB has a small crystallite size (10 nm). There was no marked change in the XRD pattern of HSB after treatment with fluoride soil solution and these results are in coincidence with results reported by Díaz-Nava et al. (2002) and Langmuir (1916).

The SEM micrographs of SB and HSB at 50.0 μm are shown in Fig. 2 (a) and 2(b), respectively. The figures show that the hydroxyapatite attaches itself to the surface of SB and constitutes rod-like structures. The elemental composition of SB was observed to change after activation with the hydroxyapatite where HSB showed extended concentration of Ca and P compared to the rest of elements projecting a change in the weight (%) of the elements within the adsorbent. Fig. 3 shows EDX analysis showing the distribution of Carbon (C), phosphorus (P), and calcium (Ca) in both SB and HSB. Unlike SB, the HSB spectra present a significant enrichment of P and Ca which are the main components of hydroxyapatite.

3.2. Fluoride adsorption

The initial experiment investigated the defluoridation efficiency of Seaweed biochar (SB) and hydroxyapatite-activated seaweed biochar (HSB) at different dosages (0.1, 0.2, 0.3, 0.4, and 0.5 g) in 5 g of fluoride-polluted soil (103.1 ± 3 mg/kg) using a 24 h contact time. The results on the influence of adsorbent dosage on fluoride removal are presented in Fig. 4(a).

As expected, the defluoridation efficiency of SB increased with increasing adsorbent dosage but the defluoridation capacity of HSB decreased with dosage which could be caused by most of the fluoride being already adsorbed at lower doses. As expected, the fluoride removal efficiency increased with increasing adsorbent dosage. The maximum defluoridation efficiency was observed at 0.5 g of HSB dosage which was 79%, 74.1% at 0.4 g, 70.8% at 0.3 g, 61.6% at 0.2 g and the least being 0.1 g with the defluoridation efficiency of 39.3%. On the other hand, SB had a defluoridation efficiency of 0.8%, 3.3%, 7.5%,
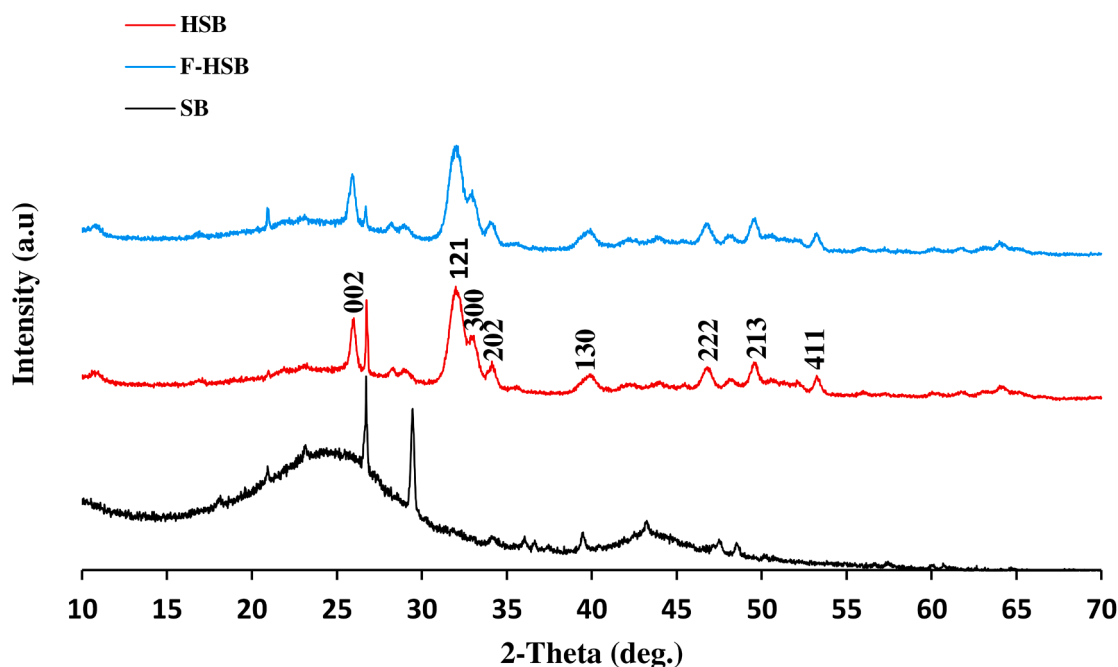

Fig. 1. The XRD pattern for SB, HSB and F-HSB conforming the formation of hydroxyapatite and its resemblance after fluoride adsorption.
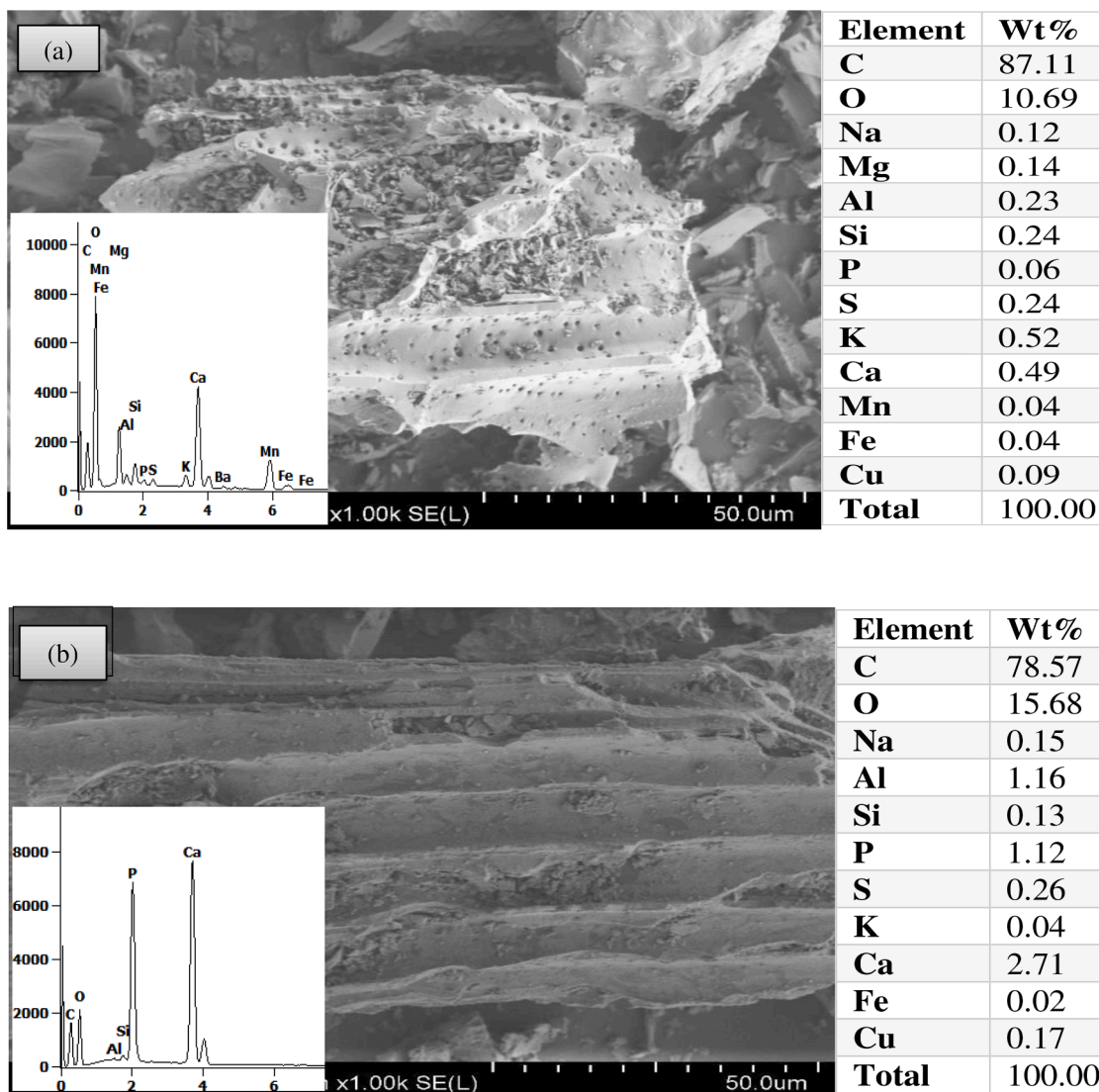
Element	Wt%
C	87.11
O	10.69
Na	0.12
Mg	0.14
Al	0.23
Si	0.24
P	0.06
S	0.24
K	0.52
Ca	0.49
Mn	0.04
Fe	0.04
Cu	0.09
Total	100.00

Element	Wt%
C	78.57
O	15.68
Na	0.15
Al	1.16
Si	0.13
P	1.12
S	0.26
K	0.04
Ca	2.71
Fe	0.02
Cu	0.17
Total	100.00

Fig. 2. The SEM micrograph and EDX spectra for (a) seaweed biochar (SB) and (b) Hydroxyapatite activated biochar (HSB) at 50.0 μm.

8.7%, and 11.5% at 0.1, 0.2,0.3, 0.4, and 0.5 g, respectively. It was obvious that HSB had a higher defluoridation capacity compared to SB and unlike SB, the HSB concentration had no linear relationship with its defluoridation efficiency.

To further determine the maximum fluoride adsorption and saturation point of the HSB, different initial fluoride concentrations were tested against a constant adsorbent dosage (0.2 g) and its results are presented in Fig. 4(b). To distinguish the amount of initial fluoride concentration, four different NaF standards were prepared (25, 50, 75, and 100 mg/L). From Fig. 4(b), It is clear that the defluoridation capacity of HSB increased with the increasing initial fluoride concentration. At the initial fluoride of 89.1 mg/kg, the defluoridation efficiency was 45.7% (C_e = 48.3 mg/kg) while at the initial fluoride concentration of 177.6 mg/kg the defluoridation efficiency increased to 53.8% (C_e = 82.2 mg/kg) without an indication of saturation.

The defluoridation efficiency of HSB was furthermore compared to the performance of other adsorbents that were tested in the contaminated soils. A comparative study is presented in Table 2. It appears that hydroxyapatite has a highest defluoridation efficiency followed fermented seaweed and HSB. The studies report that the defluoridation efficiency of these adsorbents in the soil is highly influenced by the soil properties such as pH, texture, soil ionic load and the amount of soluble-fluoride present.

3.3. Adsorption isotherms

To intensely understand the defluoridation behavior of HSB, the defluoridation data were fitted into the two common adsorption isotherm models; Langmuir and Freundlich as can be seen in Fig. 5, and the model parameters for both models are presented in Table 3. The basic assumption of the Langmuir Theory is that adsorption occurs at the homogeneous sites which are specific inside the adsorbent. Once a fluoride ion occupies that specific site no additional fluoride adsorption happens to generate monolayer adsorption (Walsh et al., 2020). This model is presented by Eq. (3):

$$1/q_e = 1/k_L Q_{max} . 1/C_e + 1/Q_{max} \tag{3}$$

Where: - Q_{max} is the maximum monolayer adsorption capacity of HSB (mg/g), KL is the Langmuir constant (L/mg), qe is the fluoride adsorption capacity (mg/g) and C_e is the equilibrium fluoride concentration in the soil (mg/kg)

On the other hand, Freundlich's Theory works in an assumption that there exists an interaction between the fluoride ions and the adsorbent sites as well as with the adsorbed fluoride ions generating the multilayer adsorption (Sundaram et al., 2008) described by the Eq. (4):

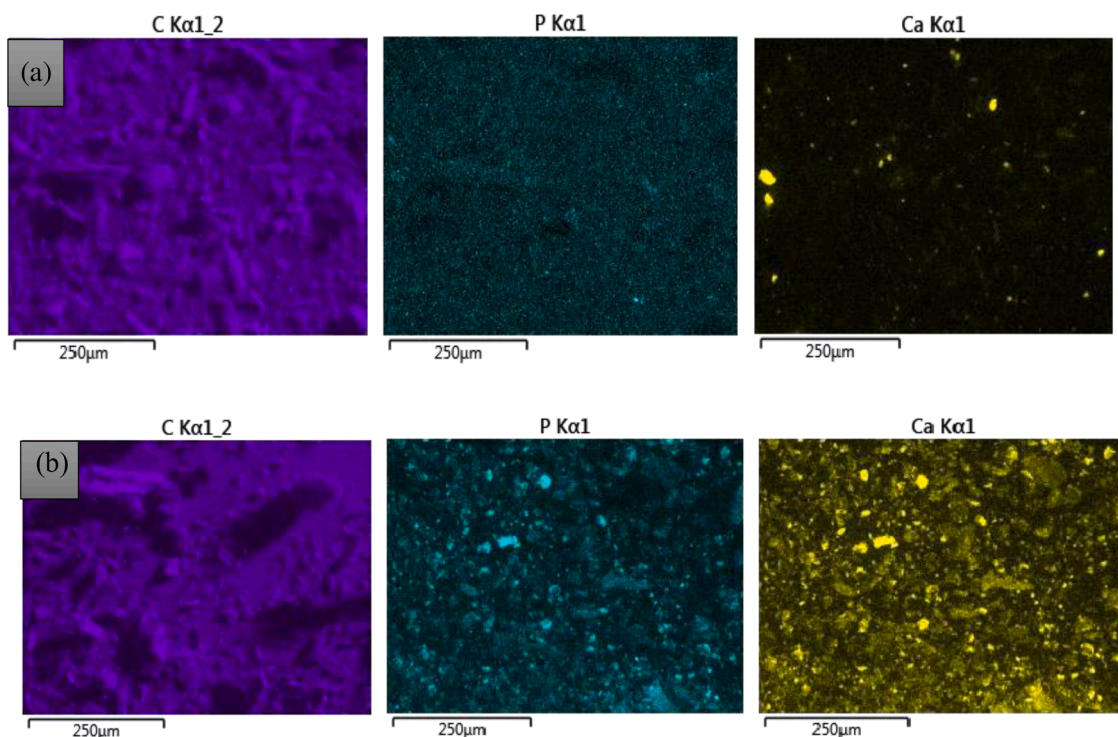$$\log q_e = \log k_f + 1/n \log Ce \tag{4}$$

Fig. 3. The EDX maps showing the spatial distribution of phosphorus and calcium in the seaweed biochar before and post-activation with hydroxyapatite(a) SB (b) HSB.
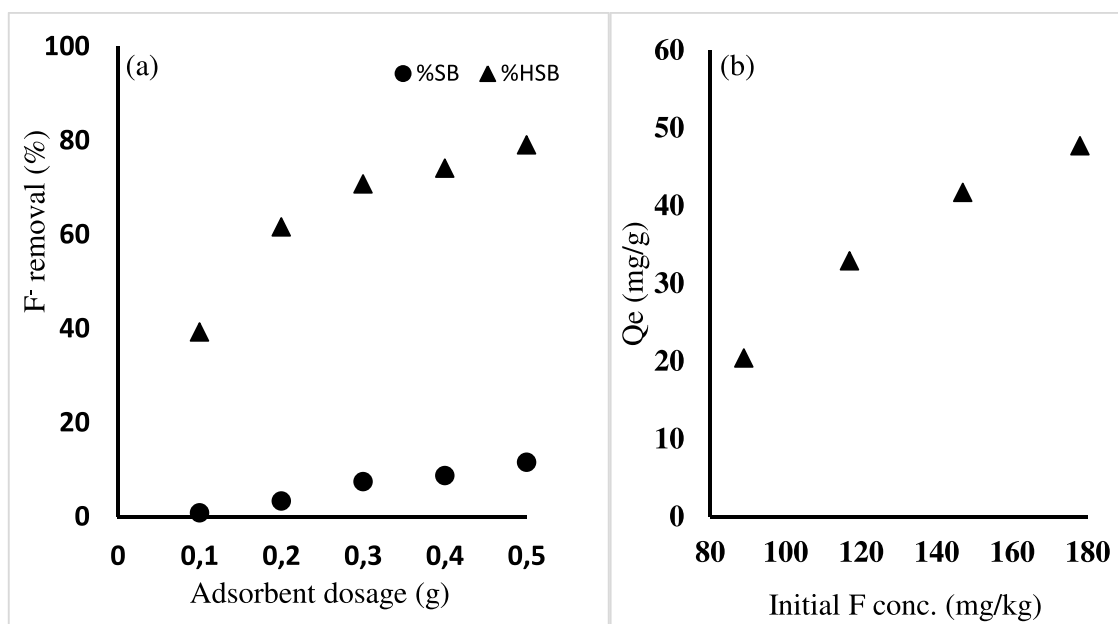

Fig. 4. (a) Comparison of the defluoridation efficiency of the seaweed biochar (SB) and the hydroxyapatite activated seaweed biochar (HSB) (b) Defluoridation capacity of the HSB at different initial fluoride concentrations using 0.2 g adsorbent.

where: - k_f is the sorption capacity of the adsorbent, and $1/n$ is the sorption intensity. The value of $1/n$ defines as to whether the adsorption process is favorable ($0.1 < 1/n < 0.5$) or unfavorable ($1/n > 2$).

Based on the correlation coefficient (R^2) results, the adsorption of fluoride onto HSB fits with the Langmuir model ($R^2 = 0.956$) followed by the Freundlich model ($R^2 = 0.942$). The obtained values of $1/n$ in the Freundlich model lie between 0 and 1 representing the favorable conditions for fluoride sorption and the value of R_L (0.85) in the Langmuir model were similarly in the range of 0 and 1 indicating favorable

fluoride adsorption conditions as well. From the experimental results, it appears that both models could be used to explain the fluoride adsorption process detected. The adsorption process was studied in a complex mixture of soil and HSB but HSB itself contains active sites from the attached hydroxyapatite as well as active sites from the seaweed biochar which were not attached to the hydroxyapatite. Therefore, the HSB adsorbent had two different active sites from hydroxyapatite and its respective seaweed biochar which could have different fluoride adsorption mechanisms exhibiting the adsorption behaviors fit to both

Table 2

A comparative study of soil fluoride removal efficiency of HSB with other reported adsorbents.

Adsorbent	F⁻ removal (%)	Refs.
Hydroxyapatite	37.3 − 87.8	(Gan et al., 2021)
Wood and bamboo charcoal	5 − 30	(Gao et al., 2012)
Fermented seaweed	47 - 85	(Moirana et al., 2022)
Al₂ (SO₄)₃	40 - 69	(Zang et al., 2022)
Hydroxyapatite-activated seaweed biochar	39 - 79	This study

Langmuir and Freundlich models. The solid phase of the soil is also a natural fluoride adsorbent providing the attachment sites for fluoride adsorption and the elemental composition of the soil provides exchange reactions with the free fluoride (Moirana et al., 2021) contributing to the existing complex adsorption mechanism of the HSB amended. Therefore, the complex nature of the adsorbent and the soil creates a complex fluoride adsorption mechanism which could either be multilayer or monolayer.

3.4. Adsorption kinetics

Fig. 6 presents the influence of contact time on fluoride adsorption on HSB. To understand the kinetics of the adsorption process, the kinetic experiments were conducted using 5 g of the soil with an initial fluoride concentration of 100.3 ± 3 mg/kg, and an adsorbent dosage of 0.2 g for contact times of 0.5, 1, 1.5, 2 and 2.5 h. Most of the fluoride was removed within the first 30 min followed by a slight removal through an equilibrium. Fluoride concentration in the soil was reduced from 100 ± 3 mg/kg to 28.8 ± 2 mg/kg equivalent to the HSB defluoridation capacity of 1.79 mg/g (71.3% removal) and the remaining 3.8 ± 1 mg/kg (2.9% removal) was removed in the subsequent 2 h accounting for a total HSB defluoridation capacity of 1.88 mg/g (75.2% removal). The defluoridation kinetics of the HSB is similar to adsorbents reported by Meenakshi and Viswanathan, (2007); Bhaumik et al., (2011); Montazeri et al., (2011). These results suggest that the saturation of HSB is reached immediately after 30 min.

According to Meenakshi and Viswanathan (2007), the defluoridation process governed by ion exchange is abrupt compared to the defluoridation process governed by adsorption (Yang and Al-Duri, 2005). The saturation point of HSB was observed past 30 min which according to

Sundaram (2008) considered not abrupt (Díaz-Nava et al., 2002) indicating both adsorption and ion-exchange processes were taking place simultaneously. The two fluoride removal processes (adsorption and ion exchange) could be attributed by the presence of active sites of both attached hydroxyapatite, unattached seaweed biochar, and the solid part of soil capable of exchanging or adsorbing the free fluoride.

The data obtained from the kinetic experiment was further fitted into the two common kinetic models; the pseudo-first (Ho, 2006) and the pseudo-second (Zhang et al., 2017) models shown by Eqs. (5) and (6). The parameters for both models are presented in Table 4.

$$Log(q_e - q_t) = log q_e - (K_1 / 2.303)t \tag{5}$$

$$t/q_t = 1/K_2 q_e^2 + (1/q_e)t \tag{6}$$

where q_t and q_e are the fluoride concentration at time (t) and at equilibrium, (mg/g) respectively.

The pseudo-first-order parameters were obtained by drawing the linear plots of ln $(q_e$-$q_t)$ Vs t whereas the pseudo-second-order parameters were obtained by drawing a linear plot of t/q_t Vs t.

The adsorption kinetics of fluoride ions into the HSB could not fit pseudo-first-order ($R^2 = 0.057$) but rather pseudo-second-order ($R^2 = 0.999$). Furthermore, the chi-square value (X^2) for the pseudo-second-order model was 0.096 which is smaller than the X^2 for the pseudo-first-order (1.74) further attests to the suitability of the pseudo-second-order to the kinetic behavior of fluoride adsorption to the HSB. On another note, the value of q_e for the pseudo-second-order (1.905 mg/g) was closer to the experimental q_e which was 2.02 mg/g whereas the q_e for the pseudo-first-order was 0.834 mg/g showing that the pseudo-first-order is not an appropriate model to describe the kinetics of HSB fluoride adsorption but rather pseudo-second-order of kinetics.

Table 3

The isotherm parameters for Langmuir and Freundlich's models describing the adsorption of fluoride on HSB.

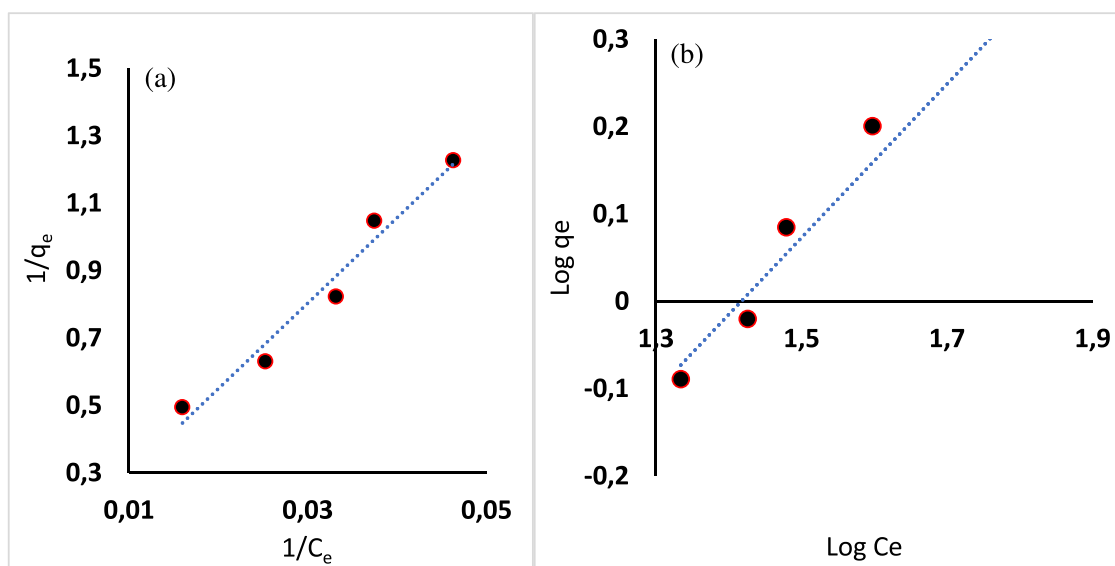|	Langmuir		Freundlich
Q (mg/g)	23.3	KF	0.0566
K_L (L/mg)	0.00169	1/n	1
R^2	0.956	R2	0.942
R_L	0.85166		

Fig. 5. The adsorption model of fluoride into HSB composite at 0.2 g adsorbent dosage (a) Langmuir (b) Freundlich.
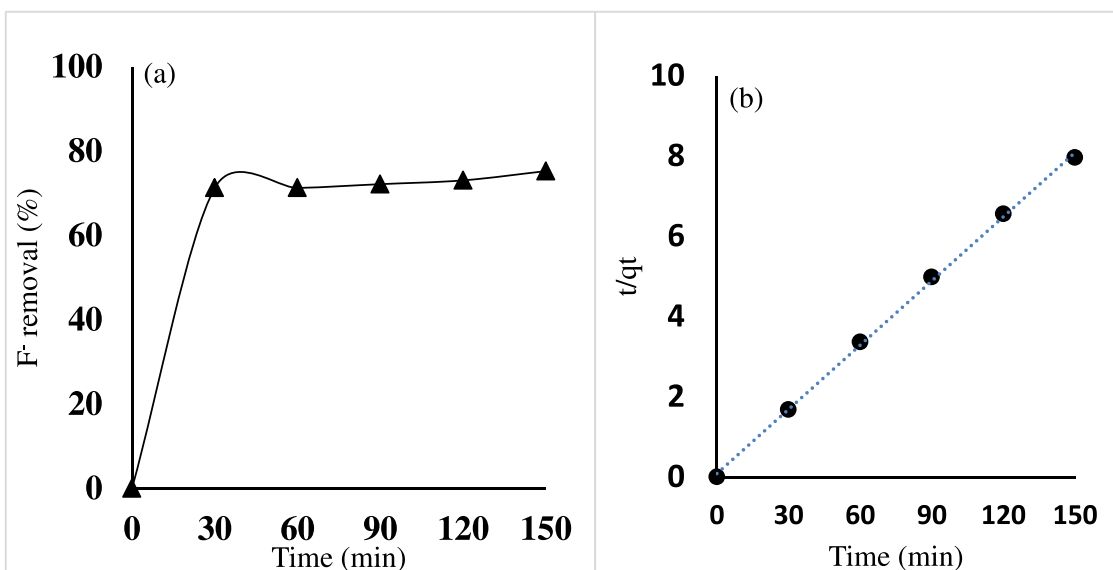
Fig. 6. (a) The kinetics of fluoride adsorption on HSB at a 0.2 g adsorbent dosage (b) The pseudo-second-order kinetics of HSB.

Table 4
Rate constants of the pseudo-first-order and pseudo-second-order.

	Pseudo-first		Pseudo-second
K_1 (/min)	-8.613E-05	K_2 (g/mg/min)	0.015119
q_e (mg/g)	0.834	q_e (mg/g)	1.9048
R^2	0.051	R^2	0.99852
X^2	1.74	X^2	0.096

3.5. Effect of pH

Fluoride adsorption is highly dependent on pH. The defluoridation efficiency of the seaweed biochar (SB) and hydroxyapatite-seaweed biochar (HSB) at five different soil pHs (3, 5, 7, 9, and 11) are presented in Fig. 7. The HSB exhibited high defluoridation efficiency over a wide range of pH (4- 11) its peak being at pH 5 – 7. The maximum defluoridation efficiency of SB was observed at pH 5 which was 37.7% and dropped abruptly to 8.4% at pH 7 hitting 0% at pH 9 and 10.2% at pH 11. Whereas the defluoridation efficiency of HSB was at its highest at pH 7 (65.5%), 5 (65.2%), 3 (53.8%), and 9 (49%) and decreased at pH 11 (37.7%) indicating a significant improvement from its respective SB. The defluoridation behavior manifested by SB was similar to the behavior of hydrous zirconium oxide which dropped from 12 mg/g at pH 5 to 2.7 mg/g at pH 7 to 0 mg/g at pH 9 (Das et al., 2003). For this study, it is presumed that most of the adsorbed fluoride at pH 5 could be adsorbed by both soil and the adsorbent as the soil is known to strongly adsorb fluoride at pH 5.5–6.5 (Hong et al., 2016) however further investigations are required.

The improved defluoridation efficiency of HSB at different pH could be contributed by the change in the surface charge of the adsorbent pH_{PZC} or by the attached hydroxyapatite. At the low pH of the soil solution, the surface of the adsorbent is protonated exerting a strong
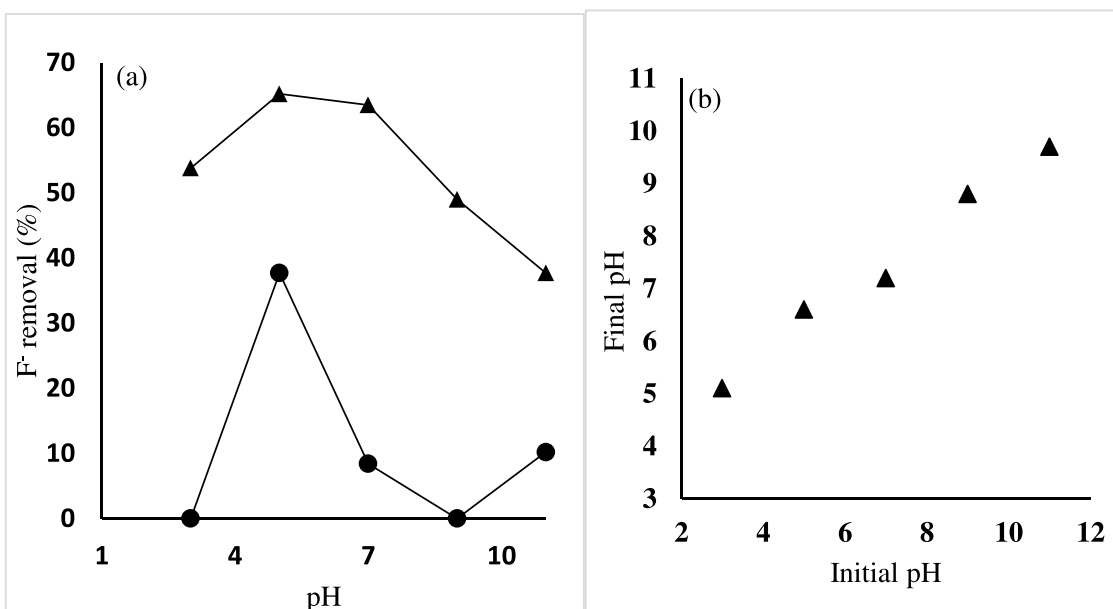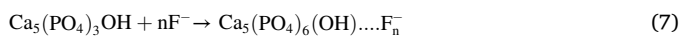

Fig. 7. (a) The impact of pH on the defluoridation capacity of activated carbon (SB) and the nanohydroxyapatite functionalized activated carbon (HSB) (b) The change of the soil pH after its amendment with the (0.2 g) HSB adsorbent.

attraction force with the negatively charged anions in the soil-solution interface. On the contrary, at high pH, the adsorbent surface acquires a negative charge exerting a repulsive force with the negatively charged soil ions. Additionally, at pH 4 – 12, hydroxyapatite exists as a stable calcium phosphate salt and therefore its -OH group can easily be exchanged with the soil anions. Although the soil solution encompasses a significant number of anions such as nitrate, phosphate, sulfate, and chlorides, hydroxyapatite displays selective adsorption towards the fluoride ions because the ionic radii of fluoride (1.33 Å) are closer to that of -OH (1.37 Å) and exchanges with fluoride to easily attain the stability of hydroxyapatite in form of fluorapatite ($Ca_5(PO_4)_3F$) which is stronger, insoluble and tougher.
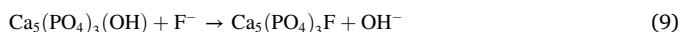
The defluoridation efficiency of adsorbents at different pH is linked to the pH_{PZC} of the adsorbent (Valdivieso et al., 2006). The pH_{ZPC} of SB was 6 and that of HSB was 7.4. The higher pH_{PZC} of HSB could be contributed by the activation of SB using hydroxyapatite. Defluoridation process is favored when the pH of the soil-water interface is less than the pH_{PZC} of the adsorbent. If the pH $<$ pH_{PZC} the surface of the adsorbent is positively charged and exerts defluoridation through chemisorption and ion-exchange which is abrupt, stable, and favors more fluoride removal. Therefore, rising the pH_{PZC} of the adsorbent enhances its defluoridation capacity (Valdivieso et al., 2006; Sundaram et al., 2009). Additionally, when the pH of the soil solution interface is higher than pH_{PZC} of the adsorbent, the surface of the adsorbent becomes negatively charged thereby exerting an electrostatic repulsion with fluoride ions. Under these conditions, defluoridation occurs through physisorption and to a lesser extent through ion exchange which is a slow and unstable process decreasing the fluoride adsorption capacity of the adsorbent. This could explain the maximum defluoridation efficiency observed at pH 5-7 followed by the sharp diminution at pH 9 – 11(McCann, 1953; Bhaumik et al., 2011). Thus, high pH_{PZC} could contribute to increased efficiency of HSB observed at a wide range of pH.

3.6. The mechanism of fluoride adsorption

The soil fluoride removal by HSB was through adsorption and ion-exchange mechanism processes (McCann, 1953). The pH_{PZC} of HSB was 7.4 and below this pH, its surface acquired a positive charge promoting maximum fluoride removal through electrostatic attraction between the positive HSB adsorbent surface and the negatively charged fluoride ions (Eqs. (7) and (8)). At pH above 7.4, the HSB surface started to acquire a negative charge reducing its affinity to the negatively charged fluoride ions and thus low defluoridation capacity derived through physisorption.

$$Ca_5(PO_4)_3OH + nF^- \rightarrow Ca_5(PO_4)_6(OH)....F_n^- \tag{7}$$

$$Ca_5(PO_4)_3OH + nF^- \rightarrow Ca_5(PO_4)_3(OH^+)...F_n^- \tag{8}$$

The ion-exchange mechanism involves the exchange with the hydroxyl (-OH) ion available in the hydroxyapatite attached to the HSB (McCann, 1953). The -OH ion exchanges with the fluoride ion available in the soil solution to form fluorapatite (Eqs. (9) and (10)). Furthermore, the soil could be a natural fluoride adsorbent at pH 5.5–6.5.

$$Ca_5(PO_4)_3(OH) + F^- \rightarrow Ca_5(PO_4)_3F + OH^- \tag{9}$$

$$Ca_5(PO_4)_3OH + F^- \rightarrow Ca_5(PO_4)_3FOH \tag{10}$$

4. Conclusion

This study investigated the efficiency of hydroxyapatite-activated seaweed-derived biochar (HSB) on fluoride removal from soils. The HSB exhibited high defluoridation efficiency over a wide range of pH (4-11) its peak being at pH 5–7. The maximum defluoridation efficiency of SB was observed at pH 5 which was 37.7% and dropped abruptly to 8.4% at pH 7 hitting 0% at pH 9 and 10.2% at pH 11. Whereas the

defluoridation efficiency of HSB was at its highest at pH 7 (65.5%), 5 (65.2%), 3 (53.8%), and 9 (49%) and decreased at pH 11 (37.7%) indicating a significant improvement from its respective SB. Activation of SB with hydroxyapatite elevated its point-zero-charge (pH_{PZC}) from 6 to 7.4 which further widened its fluoride adsorption spectra from strict acidic conditions (pH 5) to a variety of pH conditions (pH 3-11). The study envisions that the observed fluoride removal by HSB adsorbent could be through three mechanisms; biosorption into the seaweed biochar, chemisorption at pH below the pH_{PZC} of HSB, or physisorption at pH above pH_{PZC} of HSB or ion exchange with the - OH ion in the hydroxyapatite part of the HSB adsorbent. The study, therefore, highlights the potential use of the HSB to reduce fluoride content in soils with a wide range of pH (from strongly acidic to strongly alkaline soils).

CRediT authorship contribution statement

Ruth Lorivi Moirana: Investigation, Methodology, Conceptualization, Writing – original draft. **Josephine Mkunda:** Project administration, Supervision, Writing – review & editing. **Revocatus Machunda:** Methodology, Conceptualization, Supervision, Writing – review & editing. **Marcos Paradelo:** Formal analysis, Validation, Supervision, Writing – review & editing. **Kelvin Mtei:** Methodology, Conceptualization, Project administration, Writing – review & editing.

Declaration of Competing Interest

The authors declare that they have no known competing financial interests or personal relationships that could have appeared to influence the work reported in this paper.

Data availability

Data will be made available on request.

Acknowledgment

References

Arnesen, A., 1997. Availability of fluoride to plants grown in contaminated soils. Plant Soil 191, 13–25.

Bashir, M., Salmiaton, A., Nourouzi, M., Azni, I., Harun, R., 2015. Fluoride removal by chemical modification of palm kernel shell-based adsorbent: a novel agricultural waste utilization approach. Asian J. Microbial. Biotech. Environ. Sci. 17, 533–542.

Bhaumik, M., Leswifi, T.Y., Maity, A., Srinivasu, V., Onyango, M.S., 2011. Removal of fluoride from aqueous solution by polypyrrole/Fe$_3$O$_4$ magnetic nanocomposite. J. Hazard. Mater. 186, 150–159.

Chai, L., Wang, Y., Zhao, N., Yang, W., You, X., 2013. Sulfate-doped Fe$_3$O$_4$/Al$_2$O$_3$ nanoparticles as a novel adsorbent for fluoride removal from drinking water. Water Res. 47, 4040–4049.

Das, D.P., Das, J., Parida, K., 2003. Physicochemical characterization and adsorption behavior of calcined Zn/Al hydrotalcite-like compound (HTlc) towards removal of fluoride from aqueous solution. J. Colloid Interface Sci. 261, 213–220.

Díaz-Nava, C., Olguín, M., Solache-Ríos, M., 2002. Water defluoridation by Mexican heulandite–clinoptilolite. Sep. Sci. Technol. 37, 3109–3128.

Evangeline, C., Pragasam, V., 2015. Adsorptive fluoride removal from aqueous solution by using saponified orange peel residue immobilized sorbent. Int.0 J. Pharm. Bio Sci. 6.

Gan, C.D., Jia, Y.B., Yang, J.Y., 2021. Remediation of fluoride contaminated soil with nano-hydroxyapatite amendment: Response of soil fluoride bioavailability and microbial communities. J. Hazard. Mater. 405, 124694.

Gao, H., Zhang, Z., Wan, X., 2012. Influences of charcoal and bamboo charcoal amendment on soil-fluoride fractions and bioaccumulation of fluoride in tea plants. Environ. Geochem. Health 34, 551–562.

Hegde, R.M., Rego, R.M., Potla, K.M., Kurkuri, M.D., Kigga, M., 2020. Bio-inspired materials for defluoridation of water: a review. Chemosphere 253, 126657.

Ho, Y.S., 2006. Second-order kinetic model for the sorption of cadmium onto tree fern: a comparison of linear and non-linear methods. Water Res. 40, 119–125.

Hong, B.D., Joo, R.N., Lee, K.S., Lee, D.S., Rhie, J.H., Min, S.w., Song, S.G., Chung, D.Y., 2016. Fluoride in soil and plant. Korean J. Agric. Sci. 43, 522–536.

Ibrahim, Y., Abuaffan, A., Bjorvatn, K., 1995. Prevalence of dental fluorosis in Sudanese children from two villages with 0.25 and 2.56 ppm fluoride in the drinking water. Int. J. Paediatr. Dent. 5, 223–229.

Langmuir, I., 1916. The constitution and fundamental properties of solids and liquids. Part I. Solids J. Am. Chem. Soc. 38, 2221–2295.

Liang, C., Gascó, G., Fu, S., Méndez, A., Paz-Ferreiro, J., 2016. Biochar from pruning residues as a soil amendment: effects of pyrolysis temperature and particle size. Soil Tillage Res. 164, 3–10.

Malde, M.K., Maage, A., Macha, E., Julshamn, K., Bjorvatn, K., 1997. Fluoride content in selected food items from five areas in East Africa. J. Food Compos. Anal. 10, 233–245.

Marcus, Y., 1991. Thermodynamics of solvation of ions. Part 5.—Gibbs free energy of hydration at 298.15 K. J. Chem. Soc. Faraday Trans. 87, 2995–2999.

McCann, H.G., 1953. Reactions of fluoride ion with hydroxyapatite. J. Biol. Chem. 201, 247–259.

McQuaker, N.R., Gurney, M., 1977. Determination of total fluoride in soil and vegetation using an alkali fusion-selective ion electrode technique. Anal. Chem. 49, 53–56.

Meenakshi, S., Viswanathan, N., 2007. Identification of selective ion-exchange resin for fluoride sorption. J. Colloid Interface Sci. 308, 438–450.

Moirana, R.L., Mkunda, J., Paradelo, M., Machunda, R., Mtei, K., 2022. Remediation of soils contaminated by fluoride using a fermentation product of seaweed (Eucheuma cottonii). Appl. Environ. Soil Sci. 2022.

Moirana, R.L., Mkunda, J., Perez, M.P., Machunda, R., Mtei, K., 2021. The influence of fertilizers on the behavior of fluoride fractions in the alkaline soil. J. Fluor. Chem. 250, 109883.

Montazeri, N., Jahandideh, R., Biazar, E., 2011. Synthesis of fluorapatite–hydroxyapatite nanoparticles and toxicity investigations. Int. J. Nanomed. 6, 197.

Mukherjee, S., Dutta, S., Ray, S., Halder, G., 2018. A comparative study on defluoridation capabilities of biosorbents: isotherm, kinetics, thermodynamics, cost estimation, and eco-toxicological study. Environ. Sci. Pollut. Res. 25, 17473–17489.

Nehra, S., Raghav, S., Kumar, D., 2020. Biomaterial functionalized cerium nanocomposite for removal of fluoride using central composite design optimization study. Environ. Pollut. 258, 113773.

Olsson, B., 1978. Dental caries and fluorosis in Arussi province, Ethiopia. Community Dent. Oral Epidemiol. 6, 338–343.

Qiu, H., Ye, M., Zhang, M.D., Zhang, X., Zhao, Y., Yu, J., 2020. Nano-hydroxyapatite encapsulated inside an anion exchanger for efficient defluoridation of neutral and weakly alkaline water. ACS ES&T Eng. 1, 46–54.

Rizzu, M., Tanda, A., Canu, L., Masawe, K., Mtei, K., Deroma, M.A., Roggero, P.P., Seddaiu, G., 2020. Fluoride uptake and translocation in food crops grown in fluoride-rich soils. J. Sci. Food Agric. 100, 5498–5509.

Sundaram, C.S., Viswanathan, N., Meenakshi, S., 2008. Uptake of fluoride by nano-hydroxyapatite/chitosan, a bioinorganic composite. Bioresour. Technol. 99, 8226–8230.

Sundaram, C.S., Viswanathan, N., Meenakshi, S., 2009. Fluoride sorption by nano-hydroxyapatite/chitin composite. J. Hazard. Mater. 172, 147–151.

Tomar, V., Prasad, S., Kumar, D., 2014. Adsorptive removal of fluoride from aqueous media using Citrus limonum (lemon) leaf. Microchem. J. 112, 97–103.

Valdivieso, A.L., Bahena, J.R., Song, S., Urbina, R.H., 2006. Temperature effect on the zeta potential and fluoride adsorption at the α-Al$_2$O$_3$/aqueous solution interface. J. Colloid Interface Sci. 298, 1–5.

Walsh, K., Mayer, S., Rehmann, D., Hofmann, T., Glas, K., 2020. Equilibrium data and its analysis with the Freundlich model in the adsorption of arsenic (V) on granular ferric hydroxide. Sep. Purif. Technol. 243, 116704.

Yang, X., Al-Duri, B., 2005. Kinetic modeling of liquid-phase adsorption of reactive dyes on activated carbon. J. Colloid Interface Sci. 287, 25–34.

Zang, J.; Wang, N.; Huang, N.; Wang, H.; Sui, B.; Zhao, C.; Zhao, X.; Liu, J., 2022. Improved adsorption of fluorine on three typical saline-sodic soils by increasing functional groups with Al2(SO4)3 incorporation.

Zhang, X., Zhang, L., Li, Z., Jiang, Z., Zheng, Q., Lin, B., Pan, B., 2017. Rational design of antifouling polymeric nanocomposite for sustainable fluoride removal from NOM-rich water. Environ. Sci. Technol. 51, 13363–13371.

Zuo, H., Chen, L., Kong, M., Qiu, L., Lü, P., Wu, P., Yang, Y., Chen, K., 2018. Toxic effects of fluoride on organisms. Life Sci. 198, 18–24.